inventions

MDPI

Article

Development of a Human Motion Analysis System Based on Sensorized Insoles and Machine Learning Algorithms for Gait Evaluation

Diego Henrique Antunes Nascimento [1], Fabrício Anicio Magalhães [2], George Schayer Sabino [3], Renan Alves Resende [3], Maria Lúcia Machado Duarte [1] and Claysson Bruno Santos Vimieiro [1,*]

[1] Bioengineering Laboratory (LABBIO), Graduate Program in Mechanical Engineering (PPGMEC), Universidade Federal de Minas Gerais (UFMG), Belo Horizonte 31270-901, MG, Brazil
[2] Department of Biomechanics, College of Education, Health, and Human Sciences, University of Nebraska at Omaha, Omaha, NE 68182, USA
[3] Graduate Program in Rehabilitation Sciences, School of Physical Education, Physical Therapy and Occupational Therapy (EEFFTO), Universidade Federal de Minas Gerais (UFMG), Belo Horizonte 31270-901, MG, Brazil
* Correspondence: claysson@gmail.com; Tel.: +55-(31)-3409-6677

Abstract: Human gait analysis can provide an excellent source for identifying and predicting pathologies and injuries. In this respect, sensorized insoles also have a great potential for extracting gait information. This, combined with mathematical techniques based on machine learning (ML), can potentialize biomechanical analyses. The present study proposes a proof-of-concept of a system based on vertical ground reaction force (vGRF) acquisition with a sensorized insole that uses an ML algorithm to identify different patterns of vGRF and extract biomechanical characteristics that can help during clinical evaluation. The acquired data from the system was clustered by an immunological algorithm (IA) based on vGRF during gait. These clusters underwent a data mining process using the classification and regression tree algorithm (CART), where the main characteristics of each group were extracted, and some rules for gait classification were created. As a result, the system proposed was able to collect and process the biomechanical behavior of gait. After the application of IA and CART algorithms, six groups were found. The characteristics of each of these groups were extracted and verified the capability of the system to collect and process the biomechanical behavior of gait, offering verification points that can help focus during a clinical evaluation.

Keywords: biomechanics on gait; data mining; gait analysis; machine learning; smart insole

Citation: Nascimento, D.H.A.; Magalhães, F.A.; Sabino, G.S.; Resende, R.A.; Duarte, M.L.M.; Vimieiro, C.B.S. Development of a Human Motion Analysis System Based on Sensorized Insoles and Machine Learning Algorithms for Gait Evaluation. *Inventions* **2022**, *7*, 98. https://doi.org/10.3390/inventions7040098

Academic Editor: Anastasios Doulamis

Received: 23 August 2022
Accepted: 11 October 2022
Published: 21 October 2022

1. Introduction

The number of studies about biometric parameters in humans has significantly increased in the last years, mainly because of the advances in microelectronics and wearable devices. For example, the ground reaction forces (GRF) during human gait can be obtained by force plates [1], instrumented treadmills [2,3], or sensorized mats [4] or insoles [5–8]. Amongst these technologies, the sensorized insoles allow the measurement of the plantar pressures and a posteriori estimate the calculation of the GRF's vertical component (vGRF) [9,10] and how these pressures are distributed in the foot's sole during movement [11,12]. This approach permits the investigation of different movement patterns [13], and it is portable and simpler to operate than the usual force plates.

Although there are commercial options for sensorized insoles (F-scan [14], Dynafoot2 [15], Flexinfit [16]), the acquisition costs are still a factor that limits the diffusion of this technology. Another factor is that commercial insoles have a closed system by the manufacturer, making integration with other software difficult, and it is impossible to modify the insole in terms of the number, position and size of sensors. These factors encourage the development of academic prototypes [5,11,17–19] to reduce costs and have greater control

during data acquisition tests. These academic prototypes also seek to optimize the insoles' layouts [20] to improve the correlation with force plates (the "gold standard") by proposing different sensor configurations and varying the position and size of the sensors in the search for better results. However, the most academic prototypes use commercial force sensors [11,14,17,19], making the level of insole customization remain limited to the types of sensors available. In addition, some studies about the academical prototypes have poor documentation regarding the manufacturing process [17], data acquisition and processing system [15,17], and some of them do not have validation based on force plates [14,17]. Therefore, it was decided to develop a sensor that would fulfill the needs of this study. The insole developed did not use any commercial sensor, and all sensors used were customized and optimized for the application. This customization of the sensors prioritized the demands of the study, the durability of the insole and the costs of the equipment which added a degree of novelty to the equipment.

Sensorized insoles can provide gait kinetic information. Based on this information, machine learning techniques have been used to identify gait patterns for injury prevention [21,22]. The study of pattern recognition based on machine learning has already been used in kinematics [23,24], which can be referenced for applications in kinetics. Several clinical dysfunctions and overload-related injuries, such as patellofemoral syndrome or rupture of the knee's anterior cruciate ligament, have been associated with abnormal movements in the frontal plane of the foot-ankle complex [25]. Either standard or abnormal foot pronation/supination movements can be identified using mathematic techniques based on machine learning (ML) [21,26] and can be used to predict future injuries [22].

According to Slijepcevic, Djordje, et al. [27], support-vector machines (SVM) and multi-layer perceptrons (MLP) are relevant ML techniques applied to gait analysis. These algorithms have two sensitive points: supervised training and they are considered a "black box" [27]. Supervised training requires prior knowledge of the gait patterns to be recognized or classified, and this knowledge is not always available. Human movement is considered a complex system [28], and it is not always clear to define a restricted number of initial patterns based on limited variables for training the algorithm. In this case, there is a risk of adding a tendency to the algorithm and restricting the generalization ability. After training the ML algorithms (SVM and MLP), it is not possible to directly evaluate the criteria adopted to perform the classification of data, and, therefore, they are called a "black box" solution.

Therefore, this work aims to present the development of a system for measuring and analyzing the vGRF through sensorized insoles. The sensorized insole proposed has an optimized layout, presenting increased sensor area, increased acquisition rate, and a low cost. The system analysis is based on an ML algorithm to identify different patterns of vGRF's signals to extract biomechanical characteristics autonomously, without prior knowledge of the data. This work proposes implementing an unsupervised machine learning algorithm (immunological algorithm, IA) that will perform clustering of gait patterns without needing prior knowledge of the data. The response of this algorithm was used as a basis for training another algorithm (classification and regression tree, CART), from which it is possible to extract the criteria adopted to perform the classification. The interaction between IA and CART makes it possible to create a self-sufficient processing funnel capable of identifying and classifying gait patterns, providing a structured flow that underlies this answer. Hence, coaches, clinicians, and researchers can benefit from a low-cost, accurate, and user-friendly system for the clinical evaluation of walking.

2. Materials and Methods

A low-cost sensorized insole with resistive sensors was developed to obtain the gait information and build a database. An ML algorithm uses this database to seek similarities between an individual's gait characteristics to cluster them and to construct a list of rules about this classification to explore potential relations. The typical algorithm for gait clustering and classification are K-nearest neighbors [29] and support-vector machines [29].

However, these algorithms must have supervised training [30]. Because of that, the immunological algorithm (IA) was chosen to perform the previous classification to overcome this limitation. The IA [26] is an ML algorithm based on unsupervised learning. This means that prior classification knowledge of the database is not required [22]. Once the algorithm adapts to the database, it becomes convenient to use it in a complex system of limited predictability [31]. After solving the problem of identifying the initial data, the classification and regression trees (CART) algorithm was chosen to extract features (i.e., data mining) [32] and explicitly show how the clusters differ themselves considering gait's biomechanical characteristics. The CART is different from other classification algorithms such as MLP and SVM because the classification process is structured, allowing further exploration.

2.1. Insole Construction

The most popular sensorized insoles use two types of sensors: piezoelectric [33,34] and resistive [35]. Piezoelectric sensors record the pressure variation during activation, which compromises the assessment of static situations (i.e., constant pressure). Resistive sensors, on the other hand, use a conductive polymeric membrane capable of changing their conductivity when pressed. The sensorized insoles of the present study were built using resistive sensors, an electronic circuit was printed into a copper-coated polyamide blade (Figure 1a), and a conductive polymeric film was added to the pressure sensor regions (Figure 1a). In the literature, the regions of sensors' positioning (plantar mask) may vary according to the purpose of the study and are usually numbered to represent the points of interest [22].

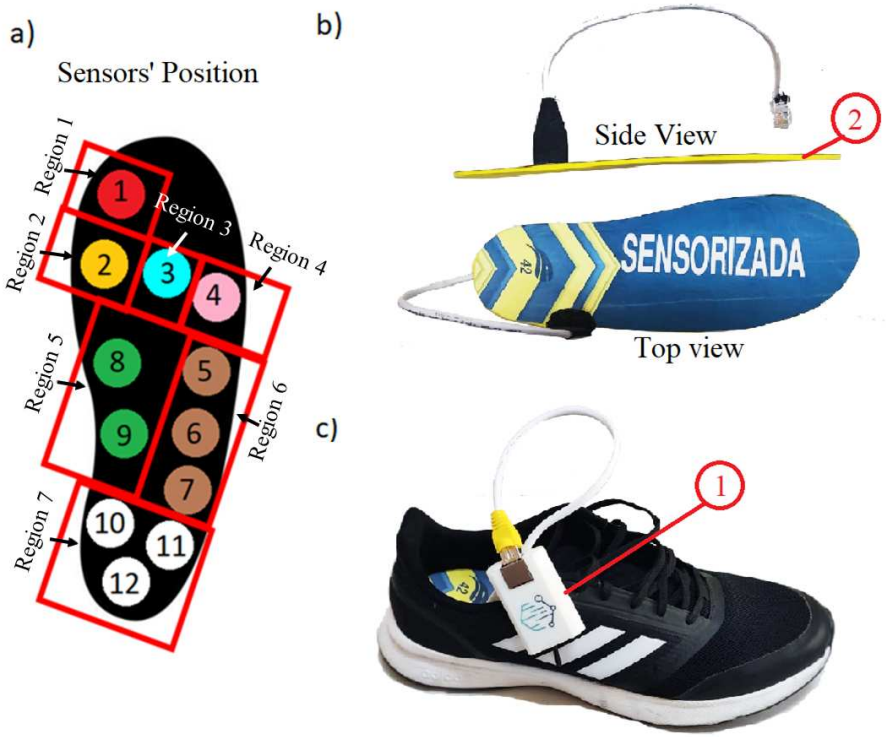

Figure 1. (**a**) Visualization of the seven regions of sensors with 12 sensors in total. (**b**) Visualization of the finished sensorized insole. The picture also shows the EVA base of the insole (2). (**c**) Visualizing the compact sender device (1) that connects with a sensorized insole using an RJ45 connector.

Seven regions were chosen to include the sensors according to the foot anatomy [20,36], and each region also has a relationship with the gait phases and their positions, which permits us to observe some behaviors of the following regions: posterior calcaneus (three sensors)—this region is the most important region to record loading response (first phase of gait); medial midfoot (navicular bone, two sensors) and lateral midfoot (cuboid bone,

three sensors)—these regions can indicate medialization of plantar pressure and may be an indicator of flat feet or increased pronation; lateral forefoot (5th metatarsal head, one sensor), central forefoot (between the second and third metatarsals heads, one sensor) and medial forefoot (1st metatarsal head, one sensor)—these regions are responsible for recording terminal support and pre-swing. The balance between these three regions indicates medialization or lateralization of plantar pressure. Finally, the last region is the hallux (1st proximal phalangeal head, one sensor). This region marks the end of the stance phase and the beginning of the swing phase.

Each insole weighs 25 g with 2.0 mm of thickness and 12 sensors. Each one has 8.05 cm^2 of area. Saidani and Salma et al. [37] report satisfactory results using insoles with 6–12 sensors, and according to Fuchs and Philip et al. [20], with 11 sensors, it is possible to achieve the "optimal compromise between simplification and measurement performance." In addition, there is a layer of EVA (ethyl vinyl acetate) shore 30 of hardness on the bottom face to protect the insole from breaking, replacing the shoes' insole and standardizing the contact between the sensorized insole and the shoe (Figure 1c). According to Klimiec et al. [26], this additional rigid layer is a "technical solution to prevent film stretching to ensure the correct measurement of forces against the substrate."

A micro-controlled circuit was built to perform the reading of each sensor through an analog port, sending a small voltage signal (3.3 V), recording and interpreting the voltage drops from their activation. The circuit was based on the ESP-32 microcontroller from the manufacturer Expressif because it has excellent processing power. The system was configured to acquire both foot data at a 375 Hz frequency, more significant than most insoles verified (Table 1), ensuring higher resolution during data acquisition. The sensor area was also bigger than usual (Table 1), helping the alignment of the anatomical regions of the foot on the sensor, a point presented as critical in the literature [20]. Both collected signals were synchronized by a router using a particular WIFI protocol from ESP-32 called espnow [38]. This protocol permits a peer-to-peer synchronization between sensors without losing the data package. After the synchronization, a router sent the information to the main computer using a serial connection to perform the data registration and post-processing using a custom-built software using C#. Table 1 shows the most popular resistive sensorized insoles in the market used for gait analysis compared to the proposed one in this study. However, the commercial systems show a high acquisition cost, stimulating many academic prototypes with novel sensor technology. Table 1 also shows some resistive instrumented insoles used for academic purposes.

Table 1. Comparison among the most popular resistive sensorized insoles.

Insoles	Number of Sensors	Freq. (Hz)	Thickness (mm)	Sensor Area (cm^2)
Proposed Insole [2]	12	375	2.00	8.05
F-Scan [1] [14]	960	750/100 (Wi-fi)	1.50	-
Dynafoot [1] [15]	58	100	-	-
Medica Flexinfit [1] [39]	214	25–50	0.30	2.27
Medilogic [1] [16]	240	50–100	1.60	-
R. Eguchi [2] [11]	14	80	-	-
Wei-Chun Hsu [2] [17]	5	100	0.45	1.27
Ivanov [2] [5]	9	25–50	0.80	0.71
A. Tiwari and D. Joshi [2] [18]	16	88	2.50	-
Guo et al. [2] [19]	8	100	-	2.62

[1]—Commercial insoles [2]—Academical insoles.

2.2. Insole Calibration

Each sensorized insole was calibrated on a bench using a precision scale (Scale SF-400, max load 10 kg/1 g, China). First, they were placed on the scale, and every single sensor was pressed using a pre-established weight of 1 kgf to 8 kgf, increasing by 1 kgf per

measurement [6]. Each measurement was performed three times to obtain an average of the measurements. Next, each cell was calibrated using linear regression to relate the captured values to the measured kgf [11] using Excel fit regression (Appendix C). Although the non-linear behavior of the electrical resistance drops of force resistive sensors is documented in the literature [40], it was observed that several authors used only the linear calibration functions [41–43], or they used the linear function as a reference for comparison, and they concluded that the linear calibration function produced superior results to non-linear functions [44,45]. This is because the acquisition system cannot measure the resistance drops directly but instead measures the generated voltage drops, which is the inverse of the resistance [40]. These voltage drops have a behavior that is nearly linear in a specific operating range that ignores very low pressures (at the beginning of deformation, where the non-linear behavior is predominant) and very high pressures (close to the sensor limit). According to the sensor calibration manual of the company TECKSCAN, the manufacturer of the (F-Scan), used as a reference, the proposed calibration function is a linear function [46]. Finally, each linear coefficient was used after calibration to adjust each sensor's time series during gait tests presented forward.

2.3. Ethical Approval

The present study was approved by the Institutional Research Ethics Committee (CAAE 00890818.8.000.5149) and conducted according to the Declaration of Helsinki.

2.4. Sample Size Calculation

To guarantee an appropriate sample size calculation and power analysis, we used G-Power (v.3.1.9.7) software [47]. The statistical test chosen on G-Power was the bivariate normal test with two tails using as a parameter Cohen's d = 0.6, α = 0.05 and power equal to 0.95 [47]. The sample size necessary was calculated to be 30 participants.

2.5. Participants

Participants with the following inclusion criteria were recruited: between 18 and 45 years old, body mass index (BMI) between 20 and 34.9 kg/m^2, no surgery on the lower limbs and lumbar spine in the last six months, and no reported neurological disorders. A total of 32 participants (18 men) were recruited during this study. Discomfort or difficulty in performing the tests was considered an exclusion criterion. Failure of equipment or data loss was also considered an exclusion criterion. All 32 participants were considered healthy. Most studies involving the validation of sensorized insoles use healthy volunteers [48] to avoid significant variations in the ground reaction curves due to a pathology that may mask or interfere with any error that the instrument may present.

2.6. Testing and Validation Process

After the calibration and signing of a free and informed consent form, each participant wore a pair of insoles and walked on the treadmill at a self-selected speed for 60 s to get used to the insole and then added 60 s for data collection.

The validity analysis was performed empirically by performing a concurrent validity analysis, in which the result of a developed instrument is compared with a "gold standard" [49]. In this way, the sensorized insoles' force estimations were compared against those from a double-belted instrumented treadmill containing two force plates (TFP) and a walking surface of 1.75 $\times$ 1 m (Bertec at 1000 Hz, Bertec Corp, Columbus, OH, USA [50]) to verify the validation of the insoles' sensors. However, there is no consensus in the literature regarding the calculation of validity [51]. The Pearson coefficient [39,52,53] is one of the most used coefficients and can be complemented with the coefficient of multiple correlations (CMC) [54,55]. According to Mukaka [56], correlation values above 0.7 are considered high correlation and, in this study, were the minimum value necessary for validation. For the validity calculation, 30 steps from all recorded steps were considered (selected by the central part, excluding the extremes), and arithmetic mean was performed to obtain a

single mean step representing the volunteer's gait. The average curves were synchronized starting based on the initial contact phase of the gait, and the acquisition frequency of the instrumented treadmill (force plate) was adjusted to the same as the sensorized insole. The raw data was filtered with a 4th order low pass Butterworth filter with a cut-off at 6 Hz for the kinematic data and 15 Hz for the kinetic data.

2.7. Pronation/Supination Classification

The kinematics were tracked in the Qualisys Track Manager program (Version 2019.3, Qualisys MEDICAL AB, Göteborg, Sweden) and processed in the Visual3D x64 Professional program (v2020.02.04, C-Motion, Germantown, MD, USA) to verify pronation and supination on the ankle join in the frontal plane during gait (Appendix B).

2.8. Immunological Algorithm (IA)

The data collected in each trial were composed of seven time series from the insoles' sensors arrangements with one minute each. Then, the vGRF could be estimated at each moment by summing all signals and applying the calibration curve (Section 2.2). In sequence, the vGRF estimated data of each lower limb (left and right) were input to the IA. This way, it was initially analyzed in 64 different walking trials (32 participants' both feet). After the tests, the IA processed the data and automatically grouped them. Each group contains samples of vGRF normalized by the maximum value (i.e., data variation was between 0 and 1). This study's magnitude of vGRF was not considered, focusing only on the waveform.

The input data underwent Fourier transform to change the domain from time to frequency. Prasanth and Hari et al. [57] reported in a systematic review that less than 5% of data analysis occurs in the frequency domain, justified by simplicity, intuitiveness, and computational complexity. Frequency domain analysis has already been applied in recognition of kinematic gait patterns [58], and it was possible to detect biometric patterns. However, according to Chockalingam, Healy, and Needham [1], the time-domain analysis is limited to the selected points on force-time graphs. However, in the frequency domain, the analysis is extended to the entire waveform, making the identification of gait abnormalities more useful [17]. Additionally, this was an attempt to represent the temporal data, decrease dimensionality to reduce the time for data processing, and standardize the problem to improve the IA results [59]. The generated Fourier coefficients represent the chromosomes of the antigens to be recognized by the immune system [30]. The silhouette criterion and the clonal selection (CLONALG) were used with a random mutation operator to evaluate the interactions based on antigen-antibody. The silhouette coefficients are the most common metric in unsupervised learning algorithms, being able to concentrate cohesion and separation metrics in a single indicator [60]. More information about this procedure is detailed in [59,61]. The IA was an authorial implementation in Visual Studio (2019, Microsoft, Redmond, WA, USA) using the open-source MathNet.Numerics package (https://numerics.mathdotnet.com/ accessed on 8 January 2022). Figure 2 presents a diagram of the grouping process.

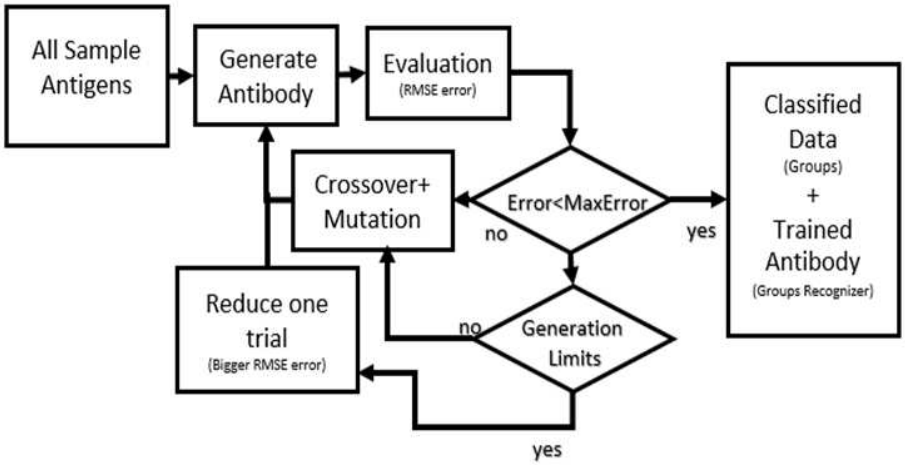

Figure 2. Data flowchart steps using IA. Each antigen-antibody interaction is evaluated using root-mean-square error to quantify this interaction sample by sample. After the evaluation process, a new group of samples is created if the mean of all RMSE is satisfactory. If the mean of all RMSE does not achieve the goal, one sample would be removed from the database, and the process is restarted until a new group is achieved. All removed samples were submitted again to the same process separately until all samples were grouped.

2.9. Classification and Regression Trees (CART)

The IA grouped the samples with similar curve shapes (based on the frequency spectrum), adding to the database new information: group classification number. After grouping, an investigative process was started to identify common characteristics that may facilitate the clinical interpretation of possible relevant issues of each group (Data Mining). In other words, a set of bioindicators used in pronation studies involving GRF was calculated for each walking phase (as described ahead), which are: mean force (MF) [62], impulse (Im) [62], the mid-lateral center of pressure axis (COPx) [63], and time duration percentage (DP) [63]. These bioindicators were extracted from the same database and were used as predictors for the training of the CART algorithm. They were statistically validated with TFP using a Student's *t*-test (paired two-sample), and the results indicated no significant difference between SI and TFP. In this process, the CART was not used to predict results but to find the bioindicator's cut-off points to define a specific group. Mean force (kgf) was calculated as the arithmetic average of vGRF registered, while impulse (kgfs) was the product of force by time on each walking phase. During walking, the impulse is related to force absorption [64]. The center of pressure (COP, in mm) was the GRF's virtual mean position acting on the foot's sole [65]. It generally starts slightly away from the posterior end of the calcaneus [66] and travels on the foot's sole during the stance phase towards the second metatarsal head [60]. This path can be calculated based on Equations (1) and (2) [7,65].

$$COP_x(t) = \frac{\sum_{i=1}^{i=7} X_i Px_i}{\sum_{i=1}^{i=7} X_i} \quad (1)$$

$$COP_y(t) = \frac{\sum_{i=1}^{i=7} X_i Py_i}{\sum_{i=1}^{i=7} X_i} \quad (2)$$

These equations use weighted averages of the sensors' positions (Px and Py) and the forces registered by the sensors (Xi), considering the center of the calcaneus as the origin of the coordinate system [65]. Thus, the COP's initial and final position in each phase could be verified, giving quantitative information for clinical assessments. For example, COP's medialization or lateralization can be used as an indicator of foot pronation or supination [30]. Finally, time duration (in percentage) was the mean time spent on each walking phase.

In sequence, the group's information from the IA was used as an outcome for the CART analysis, and the bioindicators were used as predictors. Each bioindicator was analyzed at four different moments, following the specific walking phases presented in Figure 3: loading response, midstance, propulsion (terminal stance and pre-swing), and swing [67]. These walking phases could be identified through the sequence of combined active sensors [67,68], as depicted in Figure 3. First, the loading response phase was detected when the calcaneus area achieves 2.0 kg after a period without loading (swing phase). Next, the midstance phase begins when the anterior region (central forefoot, medial forefoot, lateral, and hallux) achieves 2.0 kg and the calcaneus is still recording loading. Next, when the calcaneus stops recording, loading begins the propulsion phase (terminal stance and pre-swing). Finally, when all sensors detect no loading, the swing phase begins.

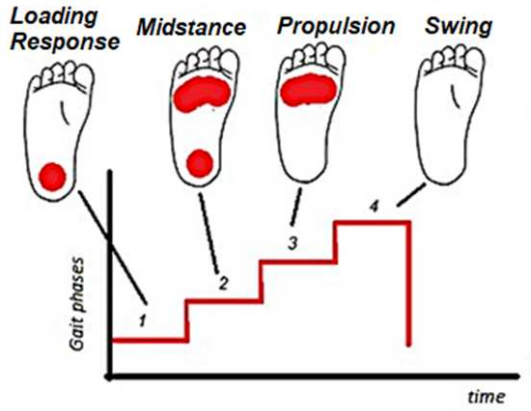

Figure 3. Walking phase identification based on activation sensor sequence. "Loading response" is based on calcaneus activation, "midstance" is based on calcaneus, lateral forefoot (5th metatarsal head), central forefoot (between the 2nd and 3rd metatarsals heads), and calcaneus activation, "Propulsion" is based on lateral forefoot (5th metatarsal head) and central forefoot (between the 2nd and 3rd metatarsals heads) activation, and "Swing" is based on no activation.

After the CART training, a decision tree was generated, and a cascade of decision rules was constructed to relate the predictors to the outcome [69,70]. This algorithm can deal with multiclass classifications and regressions and is widely used as a data extractor [1]. The attributes and similarities used to separate the groups and detect the cut-off point for each group could be identified. The CART was performed on WEKA software (version 3.8.5, University of Waikato, New Zealand). Figure 4 presents the step-by-step sequence of the data processing from the participants' test to the CART algorithm.

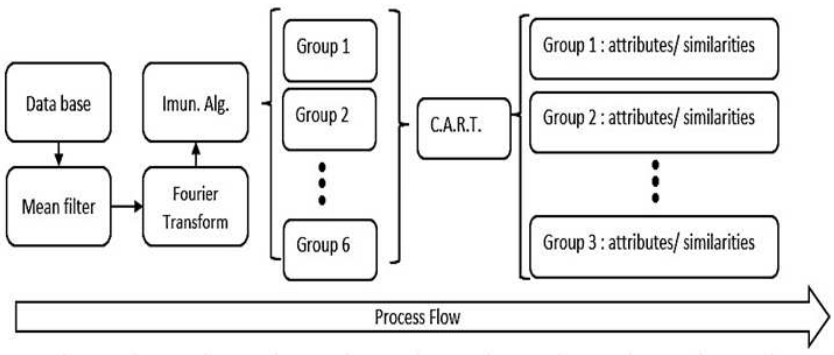

Figure 4. Data pipeline steps. All data were filtered, and a Fourier transform was applied before using the IA. As a result of IA, each sample would receive a group number based on Fourier spectrum similarities (result from IA processing). The group information was used as an outcome for the CART. After CART processing, the result was a list of N groups with similar gait behaviors.

3. Results

3.1. Insole Verification

The Person's correlation coefficient between the insoles and the scale was 0.95 (ranging from 0.93 and 0.97) for the calibration and 0.94 (ranging from 0.90 to 0.98) compared with the force plate after applying the correction factors. The smaller standard deviation was 0.15, and the greater was 0.45. Figure 5 shows two GRF's vertical components time series (insoles vs. force plate). The insole-based system had the worst performance in estimating the midstance amplitude (approximately 50% of the cycle).

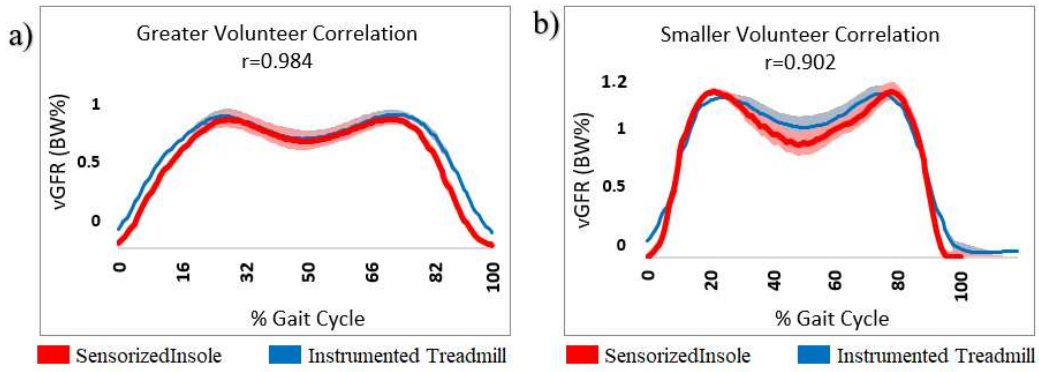

Figure 5. vGRF normalized curves dividing by maximum value during 1-min walk using the sensorized insole (red line) and the force plate (blue line) as reference. The shadows are the respective standard deviations. (**a**) Greater correlation sample and (**b**) smaller correlation sample. r: Pearson correlation coefficient.

3.2. Kinematics Evaluation

The kinematics of each sample (64 samples—32 participants, both feet) were tracked and verified on the frontal plane to classify the data into three groups: pronation, supination, and neutral on impulse phase. Figure 6 shows the normalized ankle's angle on the frontal plane representing each behavior. The pronation behavior was defined arbitrarily for analysis purposes as when the ankle's angle was smaller than −0.5 (Figure 6a) during the push-off. The supination behavior was defined as when the ankle's angle was bigger than 0.5 (Figure 6b), and the neutral was defined as when the ankle's angle was between −0.5 and 0.5 (Figure 6c).

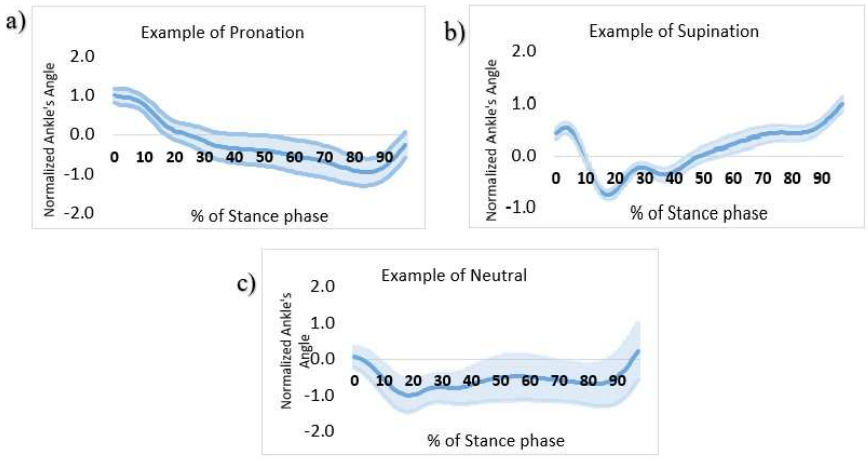

Figure 6. Normalized Ankles' Angle on the frontal plane on time, during stance phase, and with the zero references on orthostatic position. Figure (**a**) shows an example of pronation, (**b**) supination, and (**c**) neutral.

3.3. Data Processing

After applying the IA, the silhouette coefficients achieved a maximum value of 0.74 for seven groups with the following distribution of vGRF samples: 18 in Group 1, 8 in Group 2, 6 in Group 3, 6 in Group 4, 12 in Group 6, 7 in Group 6 and 7 in Group 7. The CART algorithm correctly classified samples at a rate of 86% and was considered a good result compared with the usual ML injury prediction models [21,22]. This means that 86% of samples have a unique set of features that allows the system to identify a specific behavior on walking using the bioindicators. During the training process of the CART algorithm, Group 7 was excluded because all members of Group 7 were considered errors and were removed from the analysis. This means that Group 7 could not identify a specific behavior in walking using the bioindicators.

Therefore, six groups entered the final results, with 57 trials (total without Group 7). Figure 7 shows all six groups obtained after the data processing.

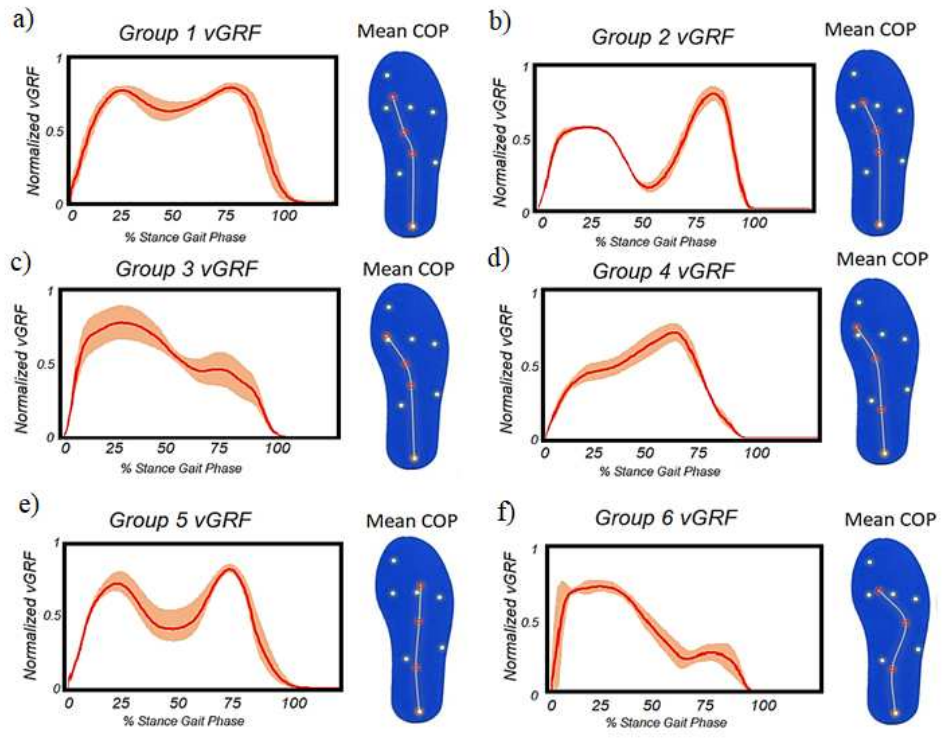

Figure 7. vGRF and COP average of each group. The continuous line is the mean of the one-minute test, and the shadows are one standard deviation of the group. The COP chart is marked with the transition of each gait: (**a**) Group 1, (**b**) Group 2, (**c**) Group 3, (**d**) Group 4, (**e**) Group 5, and (**f**) Group 6. GRF: Ground reaction force. COP: Center of pressure.

Group 1 (Figure 7a) was considered the typical group because the shape of the curve (vGRF) is similar to what is expected based on the literature [71]. In this group, an increase in the average forces during midstance (18.5%) as well as in the midstance duration (6.9% as the database average) were found. When analyzing the group members, on average, the COP had a medialization of around 22.5% in midstance. Group 1 had a prevalence of pronation (55.5%) but still had an expressive presence of supination (27.7%) and neutral (16.8%) behavior. Altered forces during the loading response were found in Groups 2, 3, and 4. Group 2 (Figure 7b) was characterized by a bigger impulse (27.4%) and average force (21.2%) during propulsion. Group 2 had a prevalence of pronation (75%) and a small presence of supination (12.5%) and neutral (12.5%) behavior. Group 3 (Figure 7c) was characterized by a decreased impulse (19.76%), mean force (5.2%), and increased loading response duration (12.7%). Group 3 had a prevalence of pronation (66.7%) and a small presence of supination (16.7%) and neutral (16.7%) behavior. Group 4 (Figure 7d) was characterized by a reduced loading response

duration (15.7%). This decreased loading response duration was accompanied by a decreased midstance duration (8.5%) and a reduced average force (20.1%). Group 4 had no pronation behavior recorded and a small presence of supination (16.7%). Neutral (83.3%) behavior dominated this group. Altered forces during the propulsion were found in Groups 5 and 6. Group 5 (Figure 7e) had an increased propulsion duration (18.7%). Group 6 (Figure 7f) was characterized by a reduced impulse (44%) and average force (37.8%), as well as decreased peak force (28.5%). In Groups 5 and 6, pronation or supination behavior was not detected. Figure 8 shows the decision-making structure extracted from CART after the pruning and exclusion of Group 7.

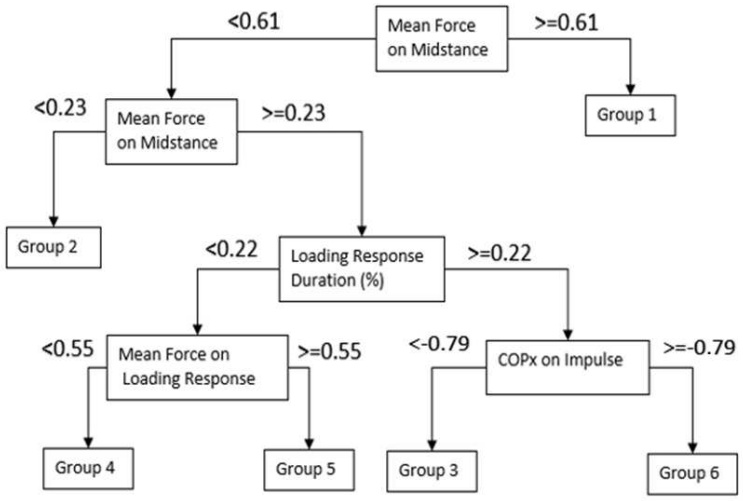

Figure 8. A flowchart of the decision-making structure extracted from CART after the pruning and exclusion of Group 7. Values of force and duration were normalized between 0 and 1, and values of COPx were normalized between −1 and 1.

4. Discussion

The aim was to develop a system to measure the vGRF and identify different patterns of vGRF signals to extract biomechanical characteristics. As a result, six groups emerged, showing particular behaviors that would help examiners to focus their attention, such as the activation of medial midfoot sensors (Group 1) and increased or decreased forces during the loading response (Groups 2, 3, and 4) and propulsion (Groups 5 and 6). Each one of these groupings may represent certain conditions, as discussed below.

The activation of medial midfoot sensors (Group 1) can represent, for example, excessive foot pronation or even the severity of flat feet. In a study about the COP path in elderly adults, a medial deviation of COP was observed, an indicator of pronation [72]. Groups 1, 2, and 3 have a predominance of pronation behavior and corroborate this relationship between COP and excessive foot pronation, although the increase in midstance mean force or activation of the medial midfoot sensors was not always present. The CART flowchart shows the opposite relationship between values of midstance mean force on Group 2 and pronation behavior. Thus, simplifying cause and effect, where a relationship of increased midstance mean force or activation of the medial midfoot sensors indicates excessive foot pronation, is reckless and is not confirmed in practice.

Altered forces or duration on the loading response phase (Groups 2, 3, and 4) can be related to gait strategies to absorb impact since increasing forces during the loading response can overload cartilages and joints [73]. Moreover, the altered forces during propulsion found in Groups 5 and 6 can result from the ankle plantar flexors' performance [73]. Although this could not be verified in the present study, these muscles are considered the most significant contributor to impulse in terms of force intensity and time duration. Therefore, any alteration in these parameters may be related to ankle plantar flexors' weakness or movement compensation [74].

Some methodological limitations could be identified, and they will be implemented in the future. Firstly, the developed sensorized insoles, similar to the commercial ones, could measure only the vertical component of GRF. The most used GRF component in the gait analysis, the anteroposterior and mediolateral axes, are crucial for quantifying the torsional forces in the lower limbs. Secondly, the system could not measure the kinematics, thus providing a complete solution for human motion analysis. Initially, it was developed to measure only the foot kinetics as their sensors, but, in the future, other devices like the inertial sensors will be added to the system. Thirdly, the sensorized insoles had the lowest accuracy in registering the plantar pressure during midstance. In this phase, the foot has a high area in contact with the ground during the gait cycle, so the area with no sensor increases its contribution to the vGRF calculations, which must be compensated for in future versions. However, even with these characteristics, the sensorized insole achieved a mean Pearson superior to 0.90, a very high positive correlation [56]. Finally, the appearance of a group of GRF patterns (Group 7) during the IA processing, for which CART could not identify patterns that differentiate them, draws attention once again to the complexity of human movement. This situation was caused by the limited amount of bioindicators available as predictors for CART, causing no related behavior patterns to be found. Different behavior patterns, such as Group 7, can be found if the number of volunteers increases or the employment of other biomarkers and, with this, a better approach will be possible.

Likewise, other factors may have impacted the results, such as the architecture of the foot arches, how tight the shoes were, and the correct placement of the insoles into the shoes. Differences in foot arches were expected, so they were not used as exclusion rules and were not considered in the analysis. A sequence of pre-tests were performed to control the tightness of shoes and correct placement of the insole. Additionally, the developed system could not identify or rank possible causes for the bioindicators' variation found in those six groups, since it was not within the scope of this study. However, it could be used to identify patterns to be deeply investigated.

The system developed could extract typical behaviors from the time series based on bioindicators from the human gait based on a database. Expanding this database with more samples can increase the number of groups to find different recognition patterns, enabling a continuous process and adaptive improvement. Although the study included only healthy volunteers, based on the inclusion, only people with neurological disorders and with a history of recent surgery were excluded, including volunteers who may have altered gait due to other factors, such as excessive pronation and supination or muscle weakness or shortening. Even in healthy volunteers, there is a presence of different gait patterns that can be used as predictors of injury [22]. Identifying gait patterns in healthy volunteers can be considered a challenge for the system [21] since the changes in gait are not as evident as in patients with neurological disorders. Sometimes, these different patterns can present themselves in different intensities and combinations, making gait analysis difficult. Therefore, the system demonstrates enough sensibility to distinguish different patterns and establish cut-off limits between different standards and can be used to investigate the potential risk of injury.

5. Conclusions

In summary, the system offered a portable and compact solution with hardware and software integration that can collect and accurately process the vGRF during walking and classify the walking behavior according to clinical groups without prior knowledge. The work's main objective was achieved. During the execution of the work, the decision to develop an authorial sensorized insole proved to be a good decision. This is because it was possible to achieve a high correlation with a force plate and high acquisition frequency using Wi-Fi data transmission to fully control the hardware and software architecture, allowing a continuous improvement of the equipment and the system. It was also possible to obtain a good finish of the product that puts the insole prototype at an advanced stage compared

to other academic prototypes regarding serial production and commercialization without depending on third-party equipment. The results of the cooperative application of machine learning techniques presented good results. The use of IA allowed a prior grouping of data based on the behavior of the vGRF without the need for prior knowledge on the researcher's part, self-regulating the number of groups that presented different characteristics from each other. The CART applied afterward allowed relating spatial-temporal variables and bioindicators to the vGRF patterns, allowing to sketch potential relationships of kinetic and kinematic behaviors. The system presented great exploratory potential and proved to be an excellent tool to improve the understanding of gait and its complexities. Furthermore, the measured biomechanical characteristics may help the foot's functional evaluation by offering quantitative parameters (bioindicators) without requiring extensive motion laboratory infrastructure and exhaustive calibration and preparation routines.

Author Contributions: Conceptualization, D.H.A.N. and G.S.S.; methodology, D.H.A.N. and G.S.S.; software, D.H.A.N.; validation, G.S.S.; formal analysis, G.S.S., D.H.A.N. and F.A.M.; investigation, D.H.A.N. and F.A.M.; writing—original draft preparation, D.H.A.N.; writing—review and editing, G.S.S., F.A.M., R.A.R., M.L.M.D. and C.B.S.V.; supervision, R.A.R., M.L.M.D. and C.B.S.V.; project administration, M.L.M.D. and C.B.S.V. All authors have read and agreed to the published version of the manuscript.

Funding: This study was financed in part by the Pró-Reitoria de Pesquisa (PRPq) from Universidade Federal de Minas Gerais (UFMG) and the Coordenação de Aperfeiçoamento de Pessoal de Nível Superior—Brasil (CAPES).

Institutional Review Board Statement: The present study was approved by the Institutional Research Ethics Committee (CAAE 00890818.8.000.5149).

Informed Consent Statement: Informed consent was obtained from all subjects involved in the study.

Data Availability Statement: Not applicable.

Acknowledgments: This study was financed in part by the Coordenação de Aperfeiçoamento de Pessoal de Nível Superior—Brasil (CAPES)—Finance Code 001 and the Pró-Reitoria de Pesquisa (PRPq) from Universidade Federal de Minas Gerais (UFMG).

Conflicts of Interest: The authors declare no conflict of interest.

Appendix A

The validation of the variables used during the study was performed using the sensorized insole together with the treadmill force platform. Each gait was collected following the same parameters adopted in the methodology. Figure A1 presents the identification of each of the variables used. Tables A1 and A2 shows the results.

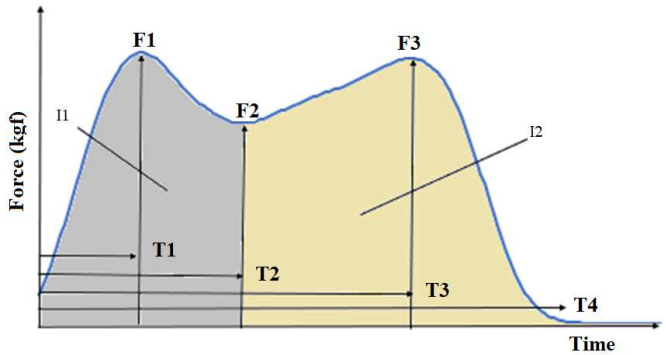

Figure A1. Identification of each of the variables used for statistical verification. Legend: I1: impulse during load absorption; F1: peak force of loading response; F2: low force of midstance; F3: peak force of push-off (impulsion); T1: time into loading response; T2: time into midstance; T3: time into impulsion; T4: total time to stance phase.

Table A1. Kinetic verification.

Localized Verification			
	RMSE	***p*-Value**	
Peak force of loading response (F1)	2.34	0.0165	
Low force of midstance (F2)	6.08	0.0760	
Peak force of push-off (F3)	5.38	0.095	
COPx (load response)	0.057	0.0432	
COPx (midstance)	0.118	0.0821	
COPx (push-off)	0.214	0.3123	
Curve Correlation			
	Pearson	RMSE	CMC
COP X	0.82	0.21	0.93
GRF	0.94	0.29	0.88

Legend: GRF: ground reaction force; COPx: center of pressure (Axis X); RMSE: root-mean-square error; CMC: coefficient of multiple correlations.

Table A2. Time Variables Verification.

	RSME	***p*-Value**
Time of Loading Response (T1)	0.01	0.04
Time of Midstance (T3-T1)	0.02	0.08
Time of Push-off (T4-T3)	0.01	0.31

Legend: RMSE: root-mean-square error.

Appendix B

For kinetic and kinematic data acquisition, 14 mm passive retro-reflective markers were fixed to each participant, seven on each individual's lower limb. The markers were positioned in the: central region of the calcaneus, head of the first metatarsal, head of the fifth metatarsal, over the lateral epicondyle of the femur, over the medial epicondyle of the femur, over the lateral malleolus, and over the medial malleolus. In addition, a rigid cluster with four passive retro-reflective markers was positioned in the posterolateral region on the distal third of the leg using an elastic band and double-sided tapes (Figure A2b —Appendix B). Data acquisition in a standing position was performed for five seconds, which was later used to create the biomechanical model and served as a biomechanical reference for the angular variations (Figure A2c —Appendix B). Subsequently, the anatomical markers on the epicondyles were removed, and gait acquisition was performed. The markers were tracked in the Qualisys Track Manager program (Version 2019.3, Qualisys MEDICAL AB, Sweden) and processed in the Visual3D x64 Professional program (v2020.02.04, C-Motion, USA). The raw data were filtered with a 4th-order low-pass Butterworth filter with a cut-off at 6 Hz for the kinematic data and 15 Hz for the kinetic data. The foot segment was modeled as a rigid cone, defined anteriorly by the metatarsal marks and posteriorly by the calcaneus mark. The leg was modeled as a rigid cylinder, defined proximally by the marks of the epicondyles and distally by the marks of the malleolus. For analysis of the movement of the ankle-foot complex, the frontal plane was considered.

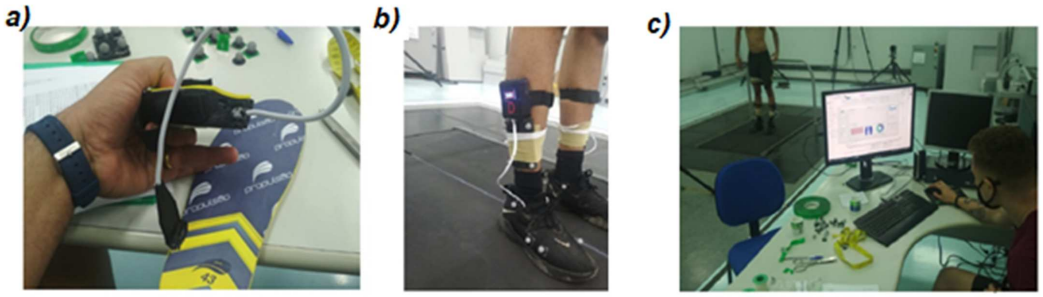

Figure A2. (**a**) Sensorized insole system for research (bigger battery). (**b**) Preparation of the participants for data acquisition with the joint use of the sensorized insole and the treadmill force plate TFP. (**c**) Data collection in a motion analysis laboratory.

As a result of data processing (vGRF and kinematics of ankle in the frontal plane), pronation behavior was considered values smaller than 0.33 in the push-off phase using the normalized ankle's angle, 0.33–0.66 was considered neutral behavior, and values greater than 0.66 were considered supination behavior. Therefore, the normalization process was conducted by dividing the values by the maximum value during the stance phase.

Appendix C

The calibration of the sensors was performed with a static load. A structure was mounted on a precision scale (Scale SF-400, max load 10 kg/1 g, Global Mix) to allow constant pressure on the sensors on the scale (Figure A3). A piston contained in the device was responsible for pressing the sensors against the scale (8 kgf maximum force), recording the simultaneous readings of the sensors and the scale and verifying the repeatability of the results and establishing a correlation equation between the signals. Figure A4 shows the calibration results for one place (the calcaneus area from an insole). Function f(x) represents the conversion of the percent of voltage drops read by the microcontroller and the load applied (X) on each senor. Each insole had its own calibration curve. All cells were tested three times, and the average was used to calibration process.

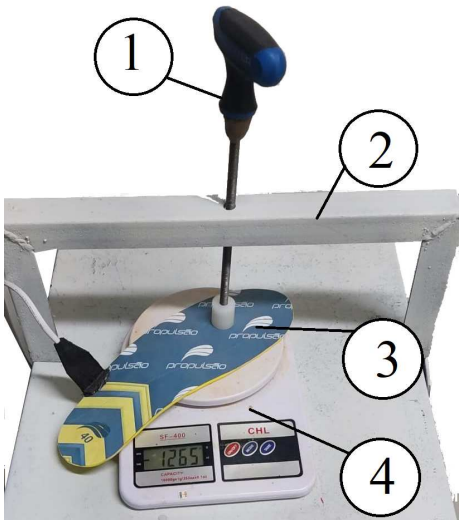

Figure A3. Device used for force dosing: 1—pressure lever; 2—fixing structure; 3—insole to be calibrated; 4—precision scale.

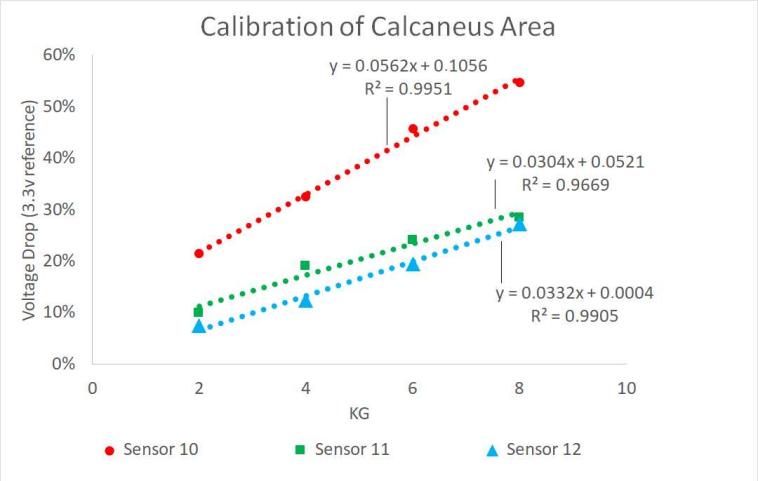

Figure A4. Calibration curve for calcaneal region sensors.

References

1. Chockalingam, N.; Healy, A.; Needham, R. Interpreting Ground Reaction Forces in Gait. In *Handbook of Human Motion*; Springer: Berlin/Heidelberg, Germany, 2016; pp. 1–5.
2. Bagesteiro, L.B.; Gould, D.; Ewins, D.J. Esteira instrumentada para medição da força de reação vertical do solo para análise de membros com próteses. *Res. Biomed. Eng.* **2011**, *27*, 3–11.
3. Vimieiro, C.; Andrada, E.; Witte, H.; Pinotti, M. A computational model for dynamic analysis of the human gait. *Comput. Methods Biomech. Biomed. Eng.* **2015**, *18*, 799–804. [CrossRef] [PubMed]
4. Middleton, L.; Buss, A.A.; Bazin, A.; Nixon, M.S. A floor sensor system for gait recognition. In Proceedings of the Fourth IEEE Workshop on Automatic Identification Advanced Technologies (AutoID'05), Buffalo, NY, USA, 17–18 October 2005; pp. 171–176.
5. Ivanov, K.; Mei, Z.; Lubich, L.; Guo, N.; Xile, D.; Zhao, Z.; Omisore, O.M.; Ho, D.; Wang, L. Design of a sensor insole for gait analysis. In Proceedings of the International Conference on Intelligent Robotics and Applications, Shenyang, China, 8–11 August 2019; Springer: Berlin/Heidelberg, Germany, 2019; pp. 433–444.
6. Malvade, P.S.; Joshi, A.K.; Madhe, S.P. In-sole Shoe Foot Pressure Monitoring for Gait Analysis. In Proceedings of the 2017 International Conference on Computing, Communication, Control and Automation (ICCUBEA), Pune, India, 17–18 August 2017; pp. 1–4.
7. Martini, E.; Fiumalbi, T.; Dell'Agnello, F.; Ivanić, Z.; Munih, M.; Vitiello, N.; Crea, S. Pressure-sensitive insoles for real-time gait-related applications. *Sensors* **2020**, *20*, 1448. [CrossRef] [PubMed]
8. Asmussen, M.J.; Kaltenbach, C.; Hashlamoun, K.; Shen, H.; Federico, S.; Nigg, B.M. Force measurements during running on different instrumented treadmills. *J. Biomech.* **2019**, *84*, 263–268. [CrossRef] [PubMed]
9. Jung, Y.; Jung, M.; Lee, K.; Koo, S. Ground reaction force estimation using an insole-type pressure mat and joint kinematics during walking. *J. Biomech.* **2014**, *47*, 2693–2699. [CrossRef] [PubMed]
10. Fong, D.T.P.; Chan, Y.Y.; Hong, Y.; Yung, P.S.H.; Fung, K.Y.; Chan, K.M. Estimating the complete ground reaction forces with pressure insoles in walking. *J. Biomech.* **2008**, *41*, 2597–2601. [CrossRef]
11. Eguchi, R.; Yorozu, A.; Fukumoto, T.; Takahashi, M. Ground reaction force estimation using insole plantar pressure measurement system from single-leg standing. In Proceedings of the 2016 IEEE International Conference on Multisensor Fusion and Integration for Intelligent Systems (MFI), Baden, Germany, 19–21 September 2016; pp. 109–113.
12. Peebles, A.T.; Ford, K.R.; Taylor, J.B.; Hart, J.M.; Sands, L.P.; Queen, R.M. Using force sensing insoles to predict kinetic knee symmetry during a stop jump. *J. Biomech.* **2019**, *95*, 109293. [CrossRef] [PubMed]
13. Hamacher, D.; Bertram, D.; Fölsch, C.; Schega, L. Evaluation of a visual feedback system in gait retraining: A pilot study. *Gait Posture* **2012**, *36*, 182–186. [CrossRef] [PubMed]
14. Tahir, A.M.; Chowdhury, M.E.; Khandakar, A.; Al-Hamouz, S.; Abdalla, M.; Awadallah, S.; Reaz, M.B.I.; Al-Emadi, N. A systematic approach to the design and characterization of a smart insole for detecting vertical ground reaction force (vGRF) in gait analysis. *Sensors* **2020**, *20*, 957. [CrossRef] [PubMed]
15. Wang, L.; Jones, D.; Chapman, G.J.; Siddle, H.J.; Russell, D.A.; Alazmani, A.; Culmer, P. A review of wearable sensor systems to monitor plantar loading in the assessment of diabetic foot ulcers. *IEEE Trans. Biomed. Eng.* **2019**, *67*, 1989–2004. [CrossRef]
16. T&T Medilogic Medizintechnik GmbH, Medilogic WLAN Insole, Schonefeld, Germany. Available online: https://medilogic.com/en/medilogic-wlan-insole/ (accessed on 23 June 2022).
17. Hsu, W.C.; Sugiarto, T.; Chen, J.W.; Lin, Y.J. The design and application of simplified insole-based prototypes with plantar pressure measurement for fast screening of flat-foot. *Sensors* **2018**, *18*, 3617. [CrossRef] [PubMed]
18. Tiwari, A.; Joshi, D. Template-based insoles for the center of pressure estimation in different foot sizes. *IEEE Sens. Lett.* **2020**, *4*, 1–4. [CrossRef]

19. Guo, R.; Cheng, X.; Hou, Z.C.; Ma, J.Z.; Zheng, W.Q.; Wu, X.M.; Jiang, D.; Pan, Y.; Ren, T.L. A Shoe-Integrated Sensor System for Long-Term Center of Pressure Evaluation. *IEEE Sens. J.* **2021**, *21*, 27037–27044. [CrossRef]
20. Fuchs, P.X.; Hsieh, C.H.; Chen, W.H.; Tang, Y.S.; Fiolo, N.J.; Shiang, T.Y. Sensor number in simplified insole layouts and the validity of ground reaction forces during locomotion. *Sport. Biomech.* **2022**, 1–14. [CrossRef] [PubMed]
21. Zhu, A.; Li, Y.; Wu, Y.; Wu, M.; Zhang, X. Locomotion mode recognition based on foot posture and ground reaction force. In Proceedings of the 2018 15th International Conference on Ubiquitous Robots (UR), Honolulu, HI, USA, 26–30 June 2018; pp. 125–129.
22. Sigurdson, H.; Chan, J.H. Machine Learning Applications to Sports Injury: A Review. In Proceedings of the 9th International Conference on Sport Sciences Research and Technology Support (icSPORTS 2021), Valletta, Malta, 28–29 October 2021; pp. 157–168.
23. Makihara, Y.; Nixon, M.S.; Yagi, Y. Gait recognition: Databases, representations, and applications. *Comput. Vis. Ref. Guide* **2020**, 1–13. [CrossRef]
24. Bouchrika, I.; Nixon, M.S. Exploratory factor analysis of gait recognition. In Proceedings of the 2008 8th IEEE International Conference on Automatic Face & Gesture Recognition, Amsterdam, The Netherlands, 17–19 September 2008; pp. 1–6.
25. Telarolli, D.J.A.; Grossi, D.B.; Cervi, A.C.C.; Santiago, P.R.P.; Lemos, T.W.; Resende, R.A. Comparison of Foot Kinematics and Foot Plantar Area and Pressure Among Five Different Closed Kinematic Tasks. *J. Am. Podiatr. Med. Assoc.* **2020**, *110*. [CrossRef]
26. Novak, D.; Reberšek, P.; De Rossi, S.M.M.; Donati, M.; Podobnik, J.; Beravs, T.; Lenzi, T.; Vitiello, N.; Carrozza, M.C.; Munih, M. Automated detection of gait initiation and termination using wearable sensors. *Med. Eng. Phys.* **2013**, *35*, 1713–1720. [CrossRef]
27. Slijepcevic, D.; Horst, F.; Lapuschkin, S.; Horsak, B.; Raberger, A.M.; Kranzl, A.; Samek, W.; Breiteneder, C.; Schöllhorn, W.I.; Zeppelzauer, M. Explaining machine learning models for clinical gait analysis. *ACM Trans. Comput. Healthc. (HEALTH)* **2021**, *3*, 1–27. [CrossRef]
28. Fonseca, S.T.; Souza, T.R.; Verhagen, E.; Van Emmerik, R.; Bittencourt, N.F.; Mendonça, L.D.; Andrade, A.G.; Resende, R.A.; Ocarino, J.M. Sports injury forecasting and complexity: A synergetic approach. *Sport. Med.* **2020**, *50*, 1757–1770. [CrossRef]
29. Potluri, S.; Chandran, A.B.; Diedrich, C.; Schega, L. Machine learning based human gait segmentation with wearable sensor platform. In Proceedings of the 2019 41st Annual International Conference of the IEEE Engineering in Medicine and Biology Society (EMBC), Berlin, Germany, 23–27 July 2019; pp. 588–594.
30. Palacio-Niño, J.O.; Berzal, F. Evaluation metrics for unsupervised learning algorithms. *arXiv* **2019**, arXiv:1905.05667.
31. Decker, L.M.; Cignetti, F.; Stergiou, N. Complexity and human gait. *Rev. Andal. Med. Deporte* **2010**, *3*, 2–12.
32. Khera, P.; Kumar, N. Role of machine learning in gait analysis: A review. *J. Med. Eng. Technol.* **2020**, *44*, 441–467. [CrossRef] [PubMed]
33. Sunarya, U.; Sun Hariyani, Y.; Cho, T.; Roh, J.; Hyeong, J.; Sohn, I.; Kim, S.; Park, C. Feature analysis of smart shoe sensors for classification of gait patterns. *Sensors* **2020**, *20*, 6253. [CrossRef]
34. Jasiewicz, B.; Klimiec, E.; Młotek, M.; Guzdek, P.; Duda, S.; Adamczyk, J.; Potaczek, T.; Piekarski, J.; Kołaszczyński, G. Quantitative analysis of foot plantar pressure during walking. *Med. Sci. Monit. Int. Med. J. Exp. Clin. Res.* **2019**, *25*, 4916. [CrossRef]
35. Dai, Y.; Xie, Y.; Chen, J.; Kang, S.; Xu, L.; Gao, S. A lamination-based piezoelectric insole gait analysis system for massive production for Internet-of-health things. *Int. J. Distrib. Sens. Netw.* **2020**, *16*, 1550147720905431. [CrossRef]
36. Klimiec, E.; Jasiewicz, B.; Piekarski, J.; Zaraska, K.; Guzdek, P.; Kołaszczyński, G. Measuring of foot plantar pressure—possible applications in quantitative analysis of human body mobility. *Meas. Sci. Technol.* **2017**, *28*, 054008. [CrossRef]
37. Saidani, S.; Haddad, R.; Mezghani, N.; Bouallegue, R. A survey on smart shoe insole systems. In Proceedings of the 2018 International Conference on Smart Communications and Networking (SmartNets), Yasmine Hammamet, Tunisia, 16–17 November 2018; pp. 1–6.
38. Pasic, R.; Kuzmanov, I.; Atanasovski, K. ESP-NOW communication protocol with ESP32. *J. Univers. Excell.* **2021**, *6*, 53–60. [CrossRef]
39. Dyer, P.S.; Bamberg, S.J.M. Instrumented insole vs. force plate: A comparison of center of plantar pressure. In Proceedings of the 2011 Annual International Conference of the IEEE Engineering in Medicine and Biology Society, Boston, MA, USA, 30 August–3 September 2011; pp. 6805–6809.
40. Dzedzickis, A.; Sutinys, E.; Bucinskas, V.; Samukaite-Bubniene, U.; Jakstys, B.; Ramanavicius, A.; Morkvenaite-Vilkonciene, I. Polyethylene-carbon composite (Velostat®) based tactile sensor. *Polymers* **2020**, *12*, 2905. [CrossRef]
41. Athavale, O.N.; Paskaranandavadivel, N.; Angeli, T.R.; Avci, R.; Cheng, L.K. Design of pressure sensor arrays to assess electrode contact pressure during in vivo recordings in the gut. In Proceedings of the 2020 42nd Annual International Conference of the IEEE Engineering in Medicine & Biology Society (EMBC), Montreal, QC, Canada, 20–24 July 2020; pp. 4204–4207.
42. Lowe, B.; Kong, Y.; Han, J. Development and application of a hand force measurement system. In Proceedings of the Proceedings of the XVIth Triennial Congress of the International Ergonomics Association, Maastricht, The Netherlands, 10–14 July 2006.
43. Ahmed, T.; Rahman, N.A.; Alam, M.K. Validation and reliability of a prototype orthodontic bracket debonding device equipped with force-sensitive resistor (FSR): A novel method of measuring orthodontic bracket debonding force in vivo. *Prog. Orthod.* **2019**, *20*, 26. [CrossRef]
44. Hopkins, M.; Vaidyanathan, R.; Mcgregor, A.H. Examination of the performance characteristics of velostat as an in-socket pressure sensor. *IEEE Sens. J.* **2020**, *20*, 6992–7000. [CrossRef]

45. Wilson, D.C.; Niosi, C.A.; Zhu, Q.A.; Oxland, T.R.; Wilson, D.R. Accuracy and repeatability of a new method for measuring facet loads in the lumbar spine. *J. Biomech.* **2006**, *39*, 348–353. [CrossRef] [PubMed]
46. Tekscan, Inc. Pressure Mapping, Force Measurement & Tactile Sensors, MA , USA. Available online: https://www.tekscan.com/sites/default/files/FLX-QS-Calibration-RevG.pdf (accessed on 7 September 2022).
47. Kang, H. Sample size determination and power analysis using the G* Power software. *J. Educ. Eval. Health Prof.* **2021**, *18*. [CrossRef] [PubMed]
48. Ngueleu, A.M.; Blanchette, A.K.; Bouyer, L.; Maltais, D.; McFadyen, B.J.; Moffet, H.; Batcho, C.S. Design and accuracy of an instrumented insole using pressure sensors for step count. *Sensors* **2019**, *19*, 984. [CrossRef] [PubMed]
49. Gopalakrishna, G.; Mustafa, R.A.; Davenport, C.; Scholten, R.J.; Hyde, C.; Brozek, J.; Schünemann, H.J.; Bossuyt, P.M.; Leeflang, M.M.; Langendam, M.W. Applying Grading of Recommendations Assessment, Development and Evaluation (GRADE) to diagnostic tests was challenging but doable. *J. Clin. Epidemiol.* **2014**, *67*, 760–768. [CrossRef] [PubMed]
50. Bertec Corporation, Instrumented Treadmills, Columbus, OH, USA. Available online: https://www.bertec.com/products/instrumented-treadmills (accessed on 7 September 2022).
51. Ferrari, A.; Cutti, A.G.; Cappello, A. A new formulation of the coefficient of multiple correlation to assess the similarity of waveforms measured synchronously by different motion analysis protocols. *Gait Posture* **2010**, *31*, 540–542. [CrossRef] [PubMed]
52. Crea, S.; Donati, M.; De Rossi, S.M.M.; Oddo, C.M.; Vitiello, N. A wireless flexible sensorized insole for gait analysis. *Sensors* **2014**, *14*, 1073–1093. [CrossRef]
53. Kanitthika, K.; Chan, K.S. Pressure sensor positions on insole used for walking analysis. In Proceedings of the The 18th IEEE International Symposium on Consumer Electronics (ISCE 2014), Jeju, Korea, 22–25 June 2014; pp. 1–2.
54. Fournier, K.A.; Amano, S.; Radonovich, K.J.; Bleser, T.M.; Hass, C.J. Decreased dynamical complexity during quiet stance in children with autism spectrum disorders. *Gait Posture* **2014**, *39*, 420–423. [CrossRef]
55. Al-Amri, M.; Nicholas, K.; Button, K.; Sparkes, V.; Sheeran, L.; Davies, J.L. Inertial measurement units for clinical movement analysis: Reliability and concurrent validity. *Sensors* **2018**, *18*, 719. [CrossRef]
56. Mukaka, M.M. A guide to appropriate use of correlation coefficient in medical research. *Malawi Med. J.* **2012**, *24*, 69–71. [PubMed]
57. Prasanth, H.; Caban, M.; Keller, U.; Courtine, G.; Ijspeert, A.; Vallery, H.; Von Zitzewitz, J. Wearable sensor-based real-time gait detection: A systematic review. *Sensors* **2021**, *21*, 2727. [CrossRef]
58. Mowbray, S.D.; Nixon, M.S. Automatic gait recognition via fourier descriptors of deformable objects. In Proceedings of the International Conference on Audio-and Video-Based Biometric Person Authentication, Guildford, UK, 9–11 June 2003; Springer: Berlin/Heidelberg, Germany, 2003; pp. 566–573.
59. Wurdeman, S.R.; Huisinga, J.M.; Filipi, M.; Stergiou, N. Multiple sclerosis affects the frequency content in the vertical ground reaction forces during walking. *Clin. Biomech.* **2011**, *26*, 207–212. [CrossRef] [PubMed]
60. Bark, C.; Chaccour, K.; Darazi, R.; El Hassani, A.H.; Andres, E. Design and development of a force-sensing shoe for gait analysis and monitoring. In Proceedings of the 2017 Fourth International Conference on Advances in Biomedical Engineering (ICABME), Beirut, Lebanon, 19–21 October 2017; pp. 1–4.
61. Cotta, C.; Hemert, J. *Evolutionary Computation in Combinatorial Optimization (7 Conf.)*; Springer: Berlin/Heidelberg, Germany, 2007.
62. Zgolli, F.; Henni, K.; Haddad, R.; Mitiche, A.; Ouakrim, Y.; Hagemeister, N.; Vendittoli, P.A.; Fuentes, A.; Mezghani, N. Kinematic data clustering for healthy knee gait characterization. In Proceedings of the 2018 IEEE Life Sciences Conference (LSC), Montreal, QC, Canada, 28–30 October 2018; pp. 239–242.
63. Brownlee, J. *Clonal Selection Theory & Clonalg—The Clonal Selection Classification Algorithm (CSCA)*; Swinburne University of Technology: Melbourne, Australia, 2005; Volume 38.
64. Farahpour, N.; Jafarnezhad, A.; Damavandi, M.; Bakhtiari, A.; Allard, P. Gait ground reaction force characteristics of low back pain patients with pronated foot and able-bodied individuals with and without foot pronation. *J. Biomech.* **2016**, *49*, 1705–1710. [CrossRef] [PubMed]
65. Resende, R.A.; Pinheiro, L.S.; Ocarino, J.M. Effects of foot pronation on the lower limb sagittal plane biomechanics during gait. *Gait Posture* **2019**, *68*, 130–135. [CrossRef] [PubMed]
66. Collins, J.; Whittle, M. Impulsive forces during walking and their clinical implications. *Clin. Biomech.* **1989**, *4*, 179–187. [CrossRef]
67. Valentina, A.; Gabriella, B.; Marco, K. Segmentation and Classification of Gait Cycles. *IEEE Trans. Neural Syst. Rehabil. Eng.* **2014**, *22*, 946–952.
68. De Rossi, S.M.; Crea, S.; Donati, M.; Reberšek, P.; Novak, D.; Vitiello, N.; Lenzi, T.; Podobnik, J.; Munih, M.; Carrozza, M.C. Gait segmentation using bipedal foot pressure patterns. In Proceedings of the 2012 4th IEEE RAS & EMBS International Conference on Biomedical Robotics and Biomechatronics (BioRob), Rome, Italy, 24–27 June 2012; pp. 361–366.
69. DeCann, B.; Ross, A.; Culp, M. On clustering human gait patterns. In Proceedings of the 2014 22nd International Conference on Pattern Recognition, Stockholm, Sweden, 24–28 August 2014; pp. 1794–1799.
70. Cutler, A.; Cutler, D.R.; Stevens, J.R. Random forests. In *Ensemble Machine Learning*; Springer: Berlin/Heidelberg, Germany, 2012; pp. 157–175.
71. Perry, J.; Araújo, A.G.N.; de Freitas, C.D.; Schoneberger, B. *Análise de Marcha*; Marcha: Sistemas de Análise de Marcha—Volume 3; Manole: Barueri, Brazil, 2005; pp 58–61.
72. Tajima, T.; Tateuchi, H.; Koyama, Y.; Ikezoe, T.; Ichihashi, N. Gait strategies to reduce the dynamic joint load in the lower limbs during a loading response in young healthy adults. *Hum. Mov. Sci.* **2018**, *58*, 260–267. [CrossRef]

73. Chiu, M.C.; Wu, H.C.; Chang, L.Y.; Wu, M.H. Center of pressure progression characteristics under the plantar region for elderly adults. *Gait Posture* **2013**, *37*, 408–412. [CrossRef]
74. Elhafez, S.M.; Ashour, A.A.; Elhafez, N.M.; Elhafez, G.M.; Abdelmohsen, A.M. Percentage contribution of lower limb moments to vertical ground reaction force in normal gait. *J. Chiropr. Med.* **2019**, *18*, 90–96. [CrossRef]